Ore Geology Reviews 92 (2018) 84–96

Contents lists available at ScienceDirect

Ore Geology Reviews

journal homepage: www.elsevier.com/locate/oregeorev

Magmatic-hydrothermal evolution of the Donggou porphyry Mo deposit at the southern margin of the North China Craton: Evidence from chemistry of biotite

Chang Jin[a,b], Xin-Yu Gao[a], Wei Terry Chen[c], Tai-Ping Zhao[a,*]

[a] Key Laboratory of Mineralogy and Metallogeny, Guangzhou Institute of Geochemistry, Chinese Academy of Sciences, Guangzhou 510640, China
[b] University of Chinese Academy of Sciences, Beijing 100039, China
[c] State Key Laboratory of Ore Deposit Geochemistry, Institute of Geochemistry, Chinese Academy of Sciences, Guiyang 550081, China

ARTICLE INFO

Keywords:
Biotite
Magmatic fluid
Halogen fugacity
Oxygen fugacity
Donggou porphyry Mo deposit

ABSTRACT

Late Mesozoic granitoids are widespread in the southern margin of the North China Craton (NCC), occurring commonly as both small porphyritic stocks and large batholiths. Most of the Mo deposits are closely associated with small porphyritic bodies. In order to determine the relationship between Mo mineralization and the granitoids, a systematic geochemical study of biotite from the Taishanmiao batholith and the Mo mineralization-associated Donggou porphyry was conducted.

Trace element features of biotites indicate a differentiation trend from rocks of the Taishanmiao batholith to those of the Donggou porphyry, as revealed by systematically decreasing K/Rb ratios, Co, Ba, V and Ti, and increasing Cs, Li, Ta and Tl. The contents of Mo also increase with the degree of magmatic differentiation.

The compositions of biotite follow a trend towards more magnesium-rich compositions, and mostly plot above the NNO buffer. The Fe^{3+}/Fe^{2+} values of biotite gradually increase from the Taishanmiao batholith to the Donggou porphyry, indicating the progressive increasing fO_2 during magmatic differentiation. The halogen fugacities of magmatic fluids calculated from biotite compositions show a trend of magmatic differentiation. The earlier fluids associated with the Taishanmiao batholith are relatively F-poor with $\log(fHF/fHCl) < 0$, whereas the later fluids derived from the Donggou porphyry are relatively F-rich with $\log(fHF/fHCl) > 0$. The high degree of melt fractionation and progressive increasing of oxygen fugacity is beneficial to concentrate Mo in the residual melt. In addition, later relatively F-rich fluid may be beneficial to extract Mo from the melt, and thus favorable for Mo mineralization.

1. Introduction

Late Mesozoic granitoid intrusions and Mo deposits are widespread in the southern margin of the North China Craton (NCC) (Mao et al., 2008, 2010). The Mo mineralization occurs inside and/or surrounding the granitoids that are considered to be the main source of molybdenum (Mao et al., 2011; Li et al., 2012a; Yang et al., 2013a, 2015; Gao et al., 2015; Wang et al., 2015). Although many granitoids including large batholiths and small porphyritic bodies are geochemically similar, most of Mo deposits are closely associated with small porphyritic bodies.

The close association between Mo mineralization and porphyry may be attributed to either magmatic or hydrothermal processes. Magmatic crystallization can cause deficit of compatible elements and enrichment of incompatible elements in residual melts (Robb, 2005). For example, Mo^{4+} has similar radius to Ti^{4+} with 0.65 and 0.605, respectively (Candela and Holland, 1986; Tacker and Candela, 1987), and thus Mo may substitute Ti in Fe- and Ti-rich minerals, such as titanite and biotite (Candela and Holland, 1986; Lowenstern et al., 1993). However, Mo^{6+} may be the predominant valence in magmas at fO_2 of Ni/NiO and above, and thus fractional crystallization will result in enrichment of Mo in residual melts (Lowenstern et al., 1993). Moreover, the sulfides may scavenge some Mo from the magma under low oxygen fugacity, whereas such an effect is limited under high oxygen fugacity. In addition, volatiles in magma can lower liquidus and solidus temperatures to promote high degrees of melt fractionation, de-polymerize the melt to stabilize Mo, and decrease viscosity to facilitate residual melt extraction and accumulation in the roof of the magma chamber (Manning, 1981; Tingle and Fenn, 1984; Dingwell, 1989; Keppler, 1993; Lowenstern et al., 1993; Bai and van Groos, 1999).

The halogen composition of fluid has an important influence on the

* Corresponding author.
E-mail address: tpzhao@gig.ac.cn (T.-P. Zhao).

https://doi.org/10.1016/j.oregeorev.2017.10.026
Received 22 March 2017; Received in revised form 12 September 2017; Accepted 31 October 2017
Available online 15 November 2017

migration and enrichment of specific elements (e.g., Keppler and Wyllie, 1991; Zajacz et al., 2008; Li and Zhou, 2015). Keppler and Wyllie (1991) found that the $D_{Mo}^{fluid/melt}$ was higher in the fluorine-containing system than that in the presence of chloride in experiments. In addition, Gunow et al. (1980) and Carten et al. (1981) proposed that fluorine may be important in the transport of molybdenum in hydrothermal systems and in the enhancement of the partitioning of molybdenum into hydrothermal fluids from silicate melt. Therefore, the abundances and speciation of fluorine and chlorine in magma and fluid are of broad interest in the field of economic geology (Coulson et al., 2001; Rasmussen and Mortensen, 2013; Zhang et al., 2016).

Previous research on Mo deposits and related granitoids in the region focused on geology and geochronology of ore deposits (Mao et al., 2008; Li et al., 2012b; Gao et al., 2013; Han et al., 2013; Wu et al., 2014), fluid inclusion and stable isotope systematics (Yang et al., 2013b, 2015; Chen et al., 2014; Li et al., 2014), and ages and sources of ore-hosting granitoids (Mao et al., 2010; Han et al., 2013; Bao et al., 2014; Gao et al., 2014a,b). Very few studies focus on the behavior of elements, particularly the Mo, in magmatic crystallization and subsequent fluid segregation processes.

Biotite is a common rock-forming mineral in granitoids, containing Ti, F and Cl. Thus, it can be a host mineral of Mo by substituting Ti. In addition, chemical composition of magmatic biotite is sensitive to chemical and physical factors associated with early magmatic through to subsequent hydrothermal stages (Abdel-Rahman, 1994; Siahcheshm et al., 2012). The classical experimental work of Wones and Eugster (1965) clearly showed that this mineral is a valuable indicator of redox conditions in granitic magmas. Wones and Eugster (1965) and Munoz (1984) also showed that the Fe/(Fe + Mg) ratio of biotite reflects the oxygen fugacity of the system, which should have a critical control on the partition behavior of Mo. In addition, in muscovite- and fluorite-free granitoid rocks, biotite contains between 70 and 90% of the F and Cl in the hydroxyl site with the remainders in apatite, amphibole and titanite (Speer, 1984), thus recording the fluorine and chlorine activities within magmas or aqueous fluids (Zhu and Sverjensky, 1991). Therefore, compositions of biotite were widely used to constrain the oxygen fugacity in magma and the halogen composition of the fluids in many types of deposits, such as porphyry Cu (Mo, Au) deposits (Selby and Nesbitt, 2000; Idrus et al., 2007; Ayati et al., 2008; Siahcheshm et al., 2012), intrusion-related Au deposits (Coulson et al., 2001; Yang and Lentz, 2005), and W (Mo, Cu) deposits (van Middelaar and Keith, 1990; Rasmussen and Mortensen, 2013; Zhang et al., 2016).

The Donggou porphyry Mo deposit is one of the largest Mo deposits in this region, containing 0.71 Mt Mo (metal) with an average grade of 0.113% (Li et al., 2007), and is spatially associated with the Taishanmiao batholiths and the Donggou porphyry. Although the Donggou deposit was commonly considered to be spatially and genetically related to the Donggou porphyry (Ye et al., 2006; Dai et al., 2009; Yang et al., 2015), it is still controversial whether the Donggou porphyry and Mo deposit are genetically related to the slightly older Taishanmiao batholiths (Ye et al., 2006; Dai et al., 2009; Huang et al., 2009). Biotite is a common mineral in both the Taishanmiao granitic batholiths and the Donggou porphyry, thus the trace elemental compositions of biotite could be used to study the behavior of Mo during magma differentiation. In this study, we conducted a systematic geochemical investigation of biotite from the Taishanmiao batholith and the Donggou porphyry, aiming to investigate the partition behavior of trace elements in biotite during magma crystallization, as well as halogen and oxygen fugacity in the magmatic-hydrothermal systems.

2. Geological setting

The Donggou porphyry Mo deposit is located in the Waifangshan area of the southern margin of the NCC. The southern margin of the NCC is generally bounded by the Sanmenxia-Lushan fault to the north and the Luonan-Luanchuan fault to the south (Fig. 1a). The main outcrop strata in the region are the Archean to Paleoproterozoic crystalline basement and the overlying late Paleoproterozoic to Phanerozoic unmetamorphosed cover sequence.

The crystalline basement is represented by the Taihua Group (2.26–2.84 Ga), which is composed of metamorphic rocks, such as amphibolite, felsic gneiss, migmatite, and metamorphosed supracrustal rocks (Kröner et al., 1988; Wan et al., 2006; Xu et al., 2009). The Xiong'er Group (1.75–1.78 Ga) is composed of mainly intermediate to acidic lavas and pyroclastic rocks intercalated with minor sedimentary rocks (< 5%), covering an area of > 60,000 km^2 (Zhao et al., 2004). The Xiong'er Group is unconformably overlain by Meso-Neoproterozoic sedimentary rocks of the Guandaokou and Luanchuan Groups that are composed mainly of carbonaceous carbonate-shale-chert. No Paleozoic-Jurassic strata can be observed in the southern margin of the NCC. Since the beginning of the Cretaceous, lacustrine or alluvial sediments began to develop in the region (Gao et al., 2014a,b).

Late Jurassic to Cretaceous magmatism characterizes the southern margin of the NCC and resulted in numerous granitoid intrusions such as the Huashan, Heyu and Taishanmiao batholiths, and Jinduicheng, Nannihu, Shangfanggou and Donggou porphyries. They emplaced in two episodes, including the Jurassic-Early Cretaceous (158 ± 3–136 ± 2 Ma) and the Early Cretaceous (134 ± 1–108 ± 2 Ma, Mao et al., 2010).

The southern margin of the NCC is one of the most important Mo ore provinces in China, with a total reserve of ca. 6 Mt Mo metal (Chen et al., 2009; Mao et al., 2011). Most of the molybdenum deposits occur as porphyry or porphyry-skarn type, and there are also minor vein type deposits. There are three pulses of Mo mineralization in the Mesozoic: 233–221 Ma, 148–138 Ma and 131–112 Ma (Mao et al., 2008), and the latter two stages of mineralization are mainly associated with porphyritic intrusions.

3. Field relationships and petrography

The Taishanmiao batholith, covering an area of 290 km^2, is one of the largest batholiths located along the southern margin of the NCC (Fig. 1b). It intruded the Paleoproterozic Xiong'er Group (1.75–1.78 Ga; Zhao et al., 2004) to the northeast and the early Cretaceous Heyu granitic pluton (148–134 Ma; Gao et al., 2010; Li et al., 2012a) to the west, and is bounded by the Checun fault to the south. Based on field occurrences, the Taishanmiao batholith can be divided into three groups as follows.

Group I, covering an area of 155 km^2, is coarse-grained syenogranite distributed in the southwest of the pluton. It consists of K-feldspar (45%–65%), plagioclase (10%–15%), quartz (25%–30%) and biotite (1%–5%), and accessory minerals including zircon, apatite, titanite and magnetite. The magmatic biotites are texturally euhedral to subhedral, with yellow-brown to green color and ranging in size from 0.4 to 2 mm (Fig. 3a). The zircon U-Pb ages of this phase vary from 131 to 121 Ma, with a weighted mean age of 125 ± 2 Ma (Gao et al., 2014a,b), which is consistent with the zircon U-Pb age of 125 ± 1 Ma by Wang et al. (2016).

Group II is medium-grained syenogranite, intruding into the Group I and covering an area of 78 km^2. It is composed of K-feldspar (35%–50%), plagioclase (10%–20%), quartz (35%) and biotite (3%), and accessory minerals such as zircon, apatite, titanite and magnetite. The magmatic biotites (0.3–1.5 mm) are euhedral to subhedral, with yellow-brown color and contain mineral inclusions of zircon and apatite (Fig. 3b). The zircons yield the U-Pb ages from 122 to 120 Ma (Qi, 2014), which is consistent with the zircon U-Pb ages (121 ± 1 Ma) by Wang et al. (2016).

Group III is porphyritic syenogranite in the northern part with an outcrop area of 56 km^2. The phenocrysts (20%) are mainly composed of quartz and perthite, while the matrix consists of fine-grained quartz, K-feldspar and minor plagioclase. The mafic mineral is mainly composed of minor biotite, and accessory minerals include zircon, apatite,

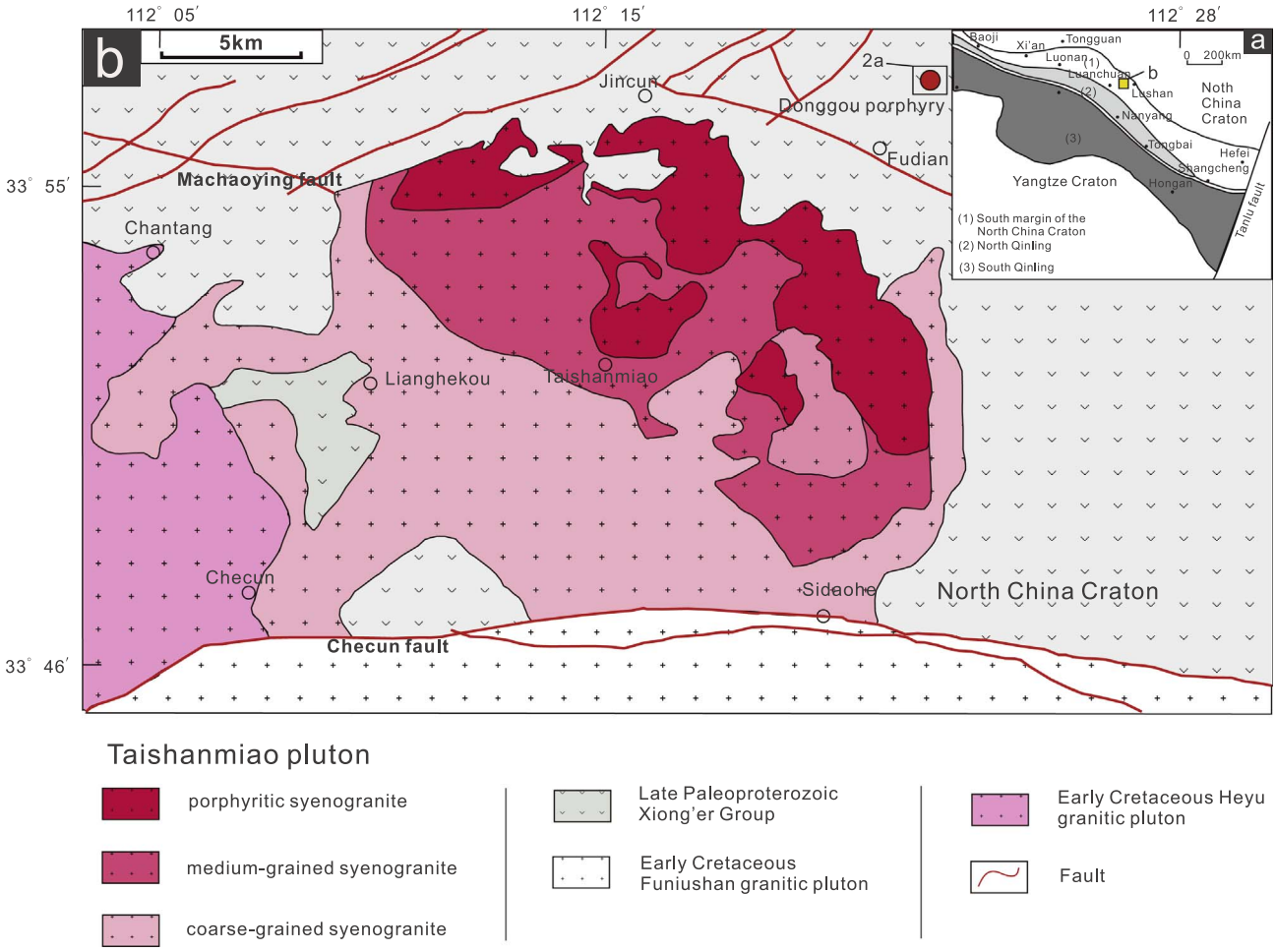

Fig. 1. (a) Simplified geological map of the Qinling Orogen Belt (modified from Gao et al., 2010); (b) Geological map of the early cretaceous granitoids in the Waifangshan area (modified from Gao et al., 2014a,b).

magnetite and fluorite. The biotites (0.5–1 mm) are euhedral to subhedral, with yellow-brown to green color (Fig. 3c). Qi (2014) reported the zircon U-Pb ages from 122 to 120 Ma. Based on zircon U-Pb ages, Group II is younger than Group I, but slightly older than Group III.

The Donggou granite porphyry is located about 7 km to the northeast of the Taishanmiao batholith, with an outcrop area of only ~0.01 km^2 (Fig. 2a). It is composed of phenocrysts of quartz, plagioclase and K-feldspar with minor biotite and accessory minerals such as magnetite, titanite, zircon and rutile. The biotites are euhedral to subhedral, 0.15–0.3 mm in length with extensive chlorite alterations. Only fresh biotite minerals were selected for geochemical analyses, especially the grains enclosed in quartz (Fig. 3d). The porphyry has LA-ICP-MS zircon U-Pb ages of 118.4 ± 0.9 Ma to 117.1 ± 0.6 Ma (Yang et al., 2013a).

The Donggou porphyry Mo deposit is spatially and genetically associated with the Donggou granite porphyry. The main Mo orebody occurs in contact zones between the porphyry and wall rocks of the Xiong'er Group, with a small part of the ore bodies within the altered porphyry (Fig. 2b). The main ore minerals are molybdenite, pyrite, chalcopyrite, galena and sphalerite. Molybdenite mainly occurs as disseminations and stockworks and is intergrown with some fluorite in the quartz–molybdenite veinlets. The main gangue minerals are quartz, feldspar, epidote, beryl, sericite, chlorite, fluorite and calcite. Hydrothermal alteration is typical of porphyry-type alteration, including potassic alteration, phyllic alteration, propylitization, carbonation and fluoritization. Re–Os isotopic analyses on molybdenite from the Donggou deposit yielded ages of 114–116 Ma (Mao et al., 2008; Ye et al., 2006).

4. Sampling and analytical methods

Biotites in three samples from each groups of the Taishanmiao batholith and the Donggou porphyry were collected and prepared for chemical analyses by electron probe microanalysis (EPMA) at the Guangzhou Institute of Geochemistry, Chinese Academy of Sciences (GIGCAS). The polished thin sections are selected carefully under the optical microscope. The analyses were conducted in wavelength-dispersion mode on a JXA JEOL-8230 probe, with a 15 kV accelerating voltage, 20 nA beam current, 1 μm beam diameter, and 20 s peak counting time for most elements (10 s for K, Na, F and Cl; 40 s for Ti and Mn). The data reduction was done using ZAF correction. Formula calculation of biotite is based on 22 atoms of oxygen by the EMPA data. The Fe^{3+} in biotite is calculated according to Dymek (1983).

The biotite grains were analyzed by laser ablation-inductively coupled plasma-mass spectrometry (LA-ICP-MS) at Nanjing FocuMS Technology Company Limited. Teledyne Cetac Technologies Analyte Excite laser-ablation system (Bozeman, Montana, USA) and Agilent Technologies 7700x quadrupole ICP-MS (Hachioji, Tokyo, Japan) were combined for the experiments. The 193 nm ArFexcimer laser, homogenized by a set of beam delivery systems, was focused on mineral surface with fluence of 6.0 J/cm^2. The laser spot size was 40 μm, with a laser repetition rate of 7 Hz. Each analysis includes a ~15 s background acquisition followed by 40 s data acquisition from the sample. Helium was applied as carrier gas to efficiently transport aerosol to ICP-MS. The SiO_2 content of each spot measured by EPMA was used with an internally-standardized data reduction scheme (Appendix Table A). Data reduction methods can be found in Liu et al. (2008). The BHVO-2G and

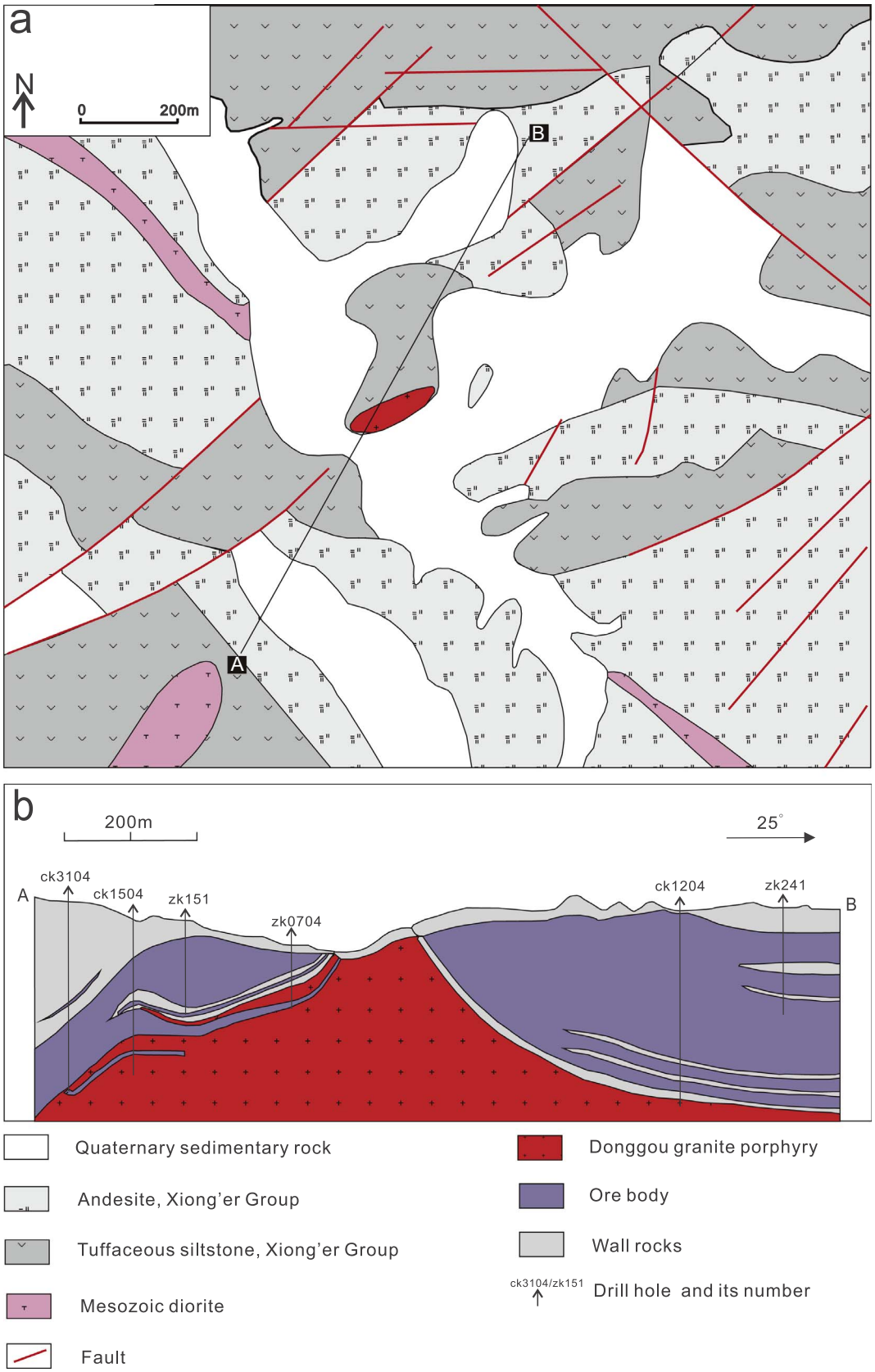

Fig. 2. (a) Simplified geological map of the Donggou Mo deposit (modified from Ye et al., 2006); (b) sketch of geological profile along A-B in Fig. 2a (modified from Fu et al., 2006).

GSE-1G glass were used as the reference material in order to confirm the precision and accuracy of the results of the LA-ICP-MS analysis. The relative standard deviations (%RSD) for the most of trace elements in BHVO-2G and GSE-1G are lower than 4% (see Appendix Table B). The relative deviations for trace elements in them are generally within 8% (see Appendix Table B).

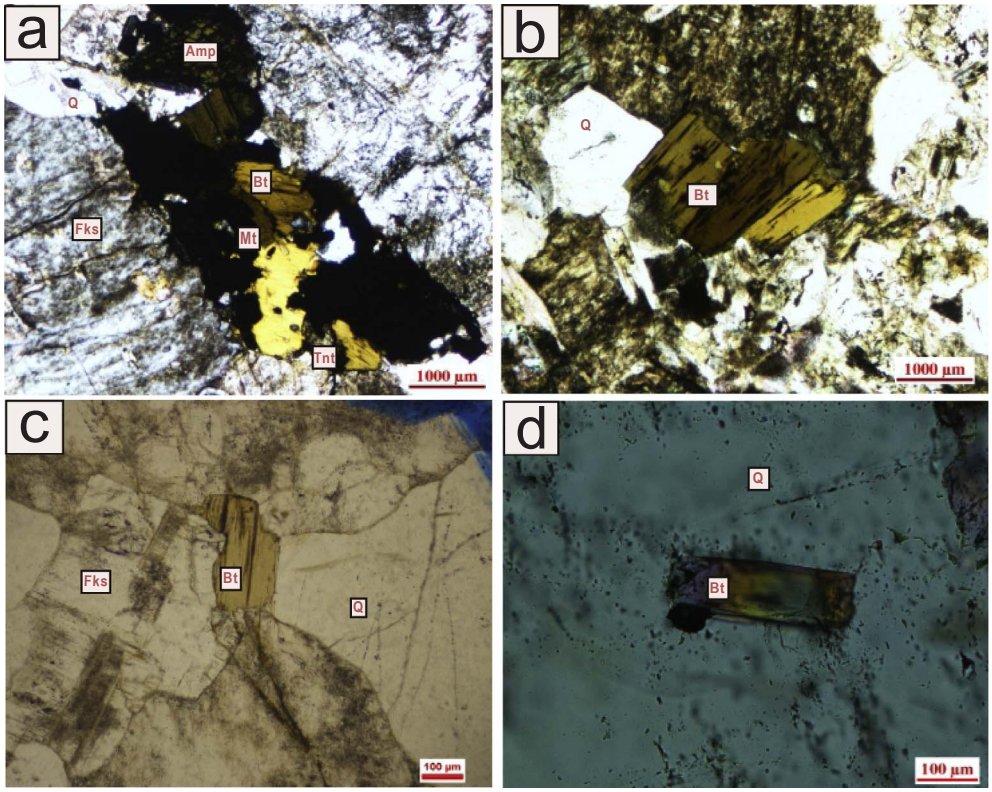

Fig. 3. Photomicrographs of biotite in Taishanmiao and Donggou plutons. (a) biotite associated with subhedral titanite, magnetite, amphibole, alkali feldspar and quartz in Group I. (b) biotite from Group II. (c) fresh magmatic biotite intergrown with alkali feldspar and quartz in Group III. (d) magmatic biotite included in quartz from Donggou porphyry. Abbreviations: Bt: biotite; Mt: magnetite; Tnt: titanite; Kfs: alkali feldspar; Amp: amphibole; Q: quartz.

5. Biotite geochemistry

5.1. Biotite classification

Only euhedral to subhedral biotites are chosen for analyses, which are most likely the primary magmatic biotites relative to the ragged secondary biotites (Rasmussen and Mortensen, 2013). In addition, TiO_2 contents can be used to distinguish primary biotite from secondary ones, because Ti content of biotite is thermally controlled (Stussi and Cuney, 1996; Patiño Douce and Harris, 1998). The biotites in this study are enriched in TiO_2 (average 2.16–3.78 wt%) (Table 1), which are similar to the magmatic biotite documented by Rasmussen and Mortensen (2013) and Zhang et al. (2016) (1.18–4.82 wt% and 1.76–4.55 wt%, respectively). According to the classification scheme of International Mineralogical Association (IMA) (Rieder et al., 1998), the trioctahedral biotites in the studied granitoids plot close to annite-phlogopite boundary, with the Fe/(Fe + Mg) ratios vary from 0.38 to 0.65 (Fig. 4a). The MgO and Fe/Fe + Mg in biotite from inter- and intra-intrusion have a good linear relation, and the chemical compositions vary systematically from Fe-rich biotite in the Taishanmiao batholith to Mg-rich biotite in the Donggou porphyry (Fig. 4b).

5.2. Trace-element characteristics

The K/Rb ratios of biotite decrease gradually from Group I (60.3–227, ave. 129), through Group II (59.8–156, ave. 91.5) and Group III (45.9–60.7, ave. 53.1), to Donggou porphyry (29.4–55.5, ave. 46.9) (Table 2, Appendix Table C, Fig. 5). The compatible elements ($D^{minerals/melt} > 1$ in felsic melts), Co (4.59–64.5 ppm), Ba (12.4–12088 ppm), V (5.62–183 ppm), and Ti (as TiO_2, 2.03–4.36%) decrease gradually from coarse-grained syenogranite (Group I), through medium-grained syenogranite (Group II), to porphyritic syenogranite (Group III) and the Donggou granite porphyry, while the incompatible elements ($D^{minerals/melt} < 1$ in felsic melts), Cs (1.29–167 ppm), Li (242–2118 ppm), Ta (1.55–52.1 ppm) and Tl (2.06–30.0 ppm) show a reversed distribution pattern and increase continuously. Mo is enriched in the Donggou porphyry (3.18–12.0 ppm) relative to the Taishanmiao batholith (0.20–4.74 ppm). Concentrations of W (0–1.64 ppm) increase gradually, whereas variations of Zn (370–1517 ppm) and Pb (2.95–60.6 ppm) are independent of K/Rb (Fig. 5, Table 2). However, biotite from the Donggou porphyry has the highest Zn and Pb contents.

6. Biotite halogen chemistry

In muscovite- and fluorite-free granitoid rocks, 70–90% of the F resides in biotite (Grabezkev et al., 1979), with the remainder in apatite and titanite (Speer, 1984). The F contents of biotite increase gradually from Group I (0.06–0.87%, ave. 0.36%), through Group II (1.19–1.47%, ave. 1.34%) and Group III (0.62–2.62%, ave. 1.86%), to the Donggou porphyry (3.59–3.75%, ave. 3.70%) (Fig. 6a and b). Relative to F, most biotites have lower Cl contents, which occupy the OH site, with Cl/(OH + F + Cl) greater than 0.1 for only a few biotites (Munoz, 1984). The Cl contents of biotites from three Groups in the Taishanmiao batholith are similar, 0.15% on average. However, the Cl contents of biotites in the Donggou porphyry are much lower (ave. 0.05%) (Fig. 6c). Biotite with high X_{Mg} incorporates more F compared to biotite with lower X_{Mg} values (Fig. 6a), a crystal-chemical effect referred to as Fe-F avoidance principle (Munoz, 1984).

The fluorine intercept [IV(F)], chlorine intercept [IV(Cl)], and F/Cl intercept [IV (F/Cl)] values are important physicochemical parameters to describe the relative degree of halogen enrichment in biotite. These values are defined by Munoz (1984) as:

$$IV(F) = 1.52X_{phl} + 0.42X_{ann} + 0.20X_{sid} - \log(X_F/X_{OH})$$

$$IV(Cl) = -5.01 - 1.93X_{phl} - \log(X_{Cl}/X_{OH})$$

$$IV(F/Cl) = IV(F) - IV(Cl)$$

where X_{phl} = Mg/sum of octahedral cations; $X_{sid} = [(3 - Si/Al)/1.75](1 - X_{phl})$; $X_{ann} = 1 - (X_{sid} + X_{phl})$. The smaller intercept value represents higher degree of halogen enrichment in biotites.

Table 1
Average chemical compositions of biotite from the felsic intrusive rocks around the Donggou Porphyry Mo deposit analyzed by electron probe microanalysis (EMPA).

Sample	Group I	Group II	Group III	Donggou granite porphyry
No. of samples	3	3	3	3
No. analyzed spots	19 ave.	16 ave.	17 ave.	12 ave.
T(K)	1021	1036	1037	1020
Na_2O	0.18	0.21	0.19	0.14
Al_2O_3	11.89	12.56	12.64	12.64
K_2O	9.38	9.46	9.29	9.88
SiO_2	36.85	37.23	37.72	39.01
MnO	0.57	0.66	0.70	1.61
MgO	9.27	12.32	12.20	13.52
CaO	0.00	0.00	0.03	0.00
FeO	23.45	18.71	19.37	15.62
TiO_2	3.53	3.48	2.34	2.23
F	0.45	1.39	2.24	3.48
Cl	0.14	0.15	0.14	0.05
F=O	0.26	0.80	1.30	2.01
Cl=O	0.11	0.12	0.11	0.04
H_2O(wt%)	3.59	3.41	3.18	2.90
total	99.10	98.96	99.07	99.59
Atom numbers calculated based on 22 (O)				
Si	5.73	5.68	5.76	5.86
Al^{IV}	2.18	2.26	2.20	2.14
T-site				
Al^{VI}	0.00	0.00	0.08	0.10
Ti	0.41	0.40	0.27	0.25
Fe^{3+}	0.44	0.48	0.51	0.51
Fe^{2+}	2.62	1.91	1.97	1.46
Mn	0.08	0.09	0.09	0.20
Mg	2.14	2.80	2.77	3.03
M-site				
Na	0.06	0.06	0.06	0.04
K	1.86	1.84	1.81	1.89
Ca	0.00	0.00	0.00	0.00
A-site				
F	0.13	0.40	0.64	0.99
Cl	0.03	0.03	0.03	0.01
OH	3.84	3.57	3.33	3.00
Fe^{3+}/Fe^{2+}	0.18	0.25	0.26	0.35
X_{Mg}	0.41	0.54	0.53	0.61
X_{sid}	0.12	0.13	0.13	0.09
X_{ann}	0.46	0.33	0.35	0.31
IV(F)	2.47	1.94	1.71	1.55
IV(Cl)	−3.66	−4.00	−3.97	−3.64
log(fH_2O/fHF)	4.80	4.18	4.00	3.82
log($fH_2O/fHCl$)	3.76	3.58	3.60	4.05
log($fHF/fHCl$)	−1.05	−0.60	−0.40	0.23

Notes: OH is calculated by OH = 4 − (Cl + F). Intercept values IV(F) and IV(Cl) and halogen fugacity are calculated by Munoz (1984).T_{Zr} were calculated by Watson and Harrison (1983).

Biotite compositions from the Taishanmiao batholith and the Donggou porphyry are shown in Fig. 6d, plotted with respect to IV(F) vs. IV(F/Cl). The diagram shows a positive correlation, with the lowest IV(F) value of biotite in the Donggou porphyry. Loferski and Ayuso (1995) proposed that the decrease of IV(F) values might be caused by crystal fractionation during which F concentrates in the late magmatic stage. In X_{Mg} vs. log(F/OH), and X_{Mg} vs. log(Cl/OH) plots, they also have a liner trend (Fig. 6b and c). In the IV(F)-IV(F/Cl) diagram (Fig. 6d), biotites from the Donggou porphyry have more remarkable F enrichments, which is similar to that of the other Porphyry Mo deposits.

7. Halogen fugacity of associated fluids

The contents of fluorine and chlorine in biotite have been used to calculate halogen fugacity of associated magma or fluids (Loferski and Ayuso, 1995; Yang and Lentz, 2005; Idrus et al., 2007; Ayati et al., 2008; Siahcheshm et al., 2012; Rasmussen and Mortensen, 2013; Zhang et al., 2016). The fugacity ratios were calculated using the equations of Munoz (1992), which are based on the revised coefficients for F-Cl-OH partitioning between biotite and hydrothermal fluids (Zhu and Sverjensky, 1991, 1992). These equations are:

$$\log(fH_2O/fHF)^{fluid} = 1000/T(2.37 + 1.1X_{phl}) + 0.43 - \log(X_F/X_{OH})^{biotite}$$

$$\log(fH_2O/fHCl)^{fluid} = 1000/T(1.15 - 0.55X_{phl}) + 0.68 - \log(X_{Cl}/X_{OH})^{biotite}$$

$$\log(fHF/fHCl)^{fluid} = -1000/T(1.22 + 1.65X_{phl}) + 0.25 + \log(X_F/X_{Cl})^{biotite}$$

where X_F, X_{Cl}, and X_{OH} are the mole fractions of F, Cl, and OH in the hydroxyl site of the biotite, and T is the temperature in Kelvin of the halogen exchange. For the temperature, we use the zircon-saturation temperatures.

The zircon saturation temperatures of the Taishanmiao batholith and Donggou porphyry vary from 716 to 799 °C (Table 1) (Gao et al., 2014a,b). The calculated log($fH_2O/fHCl$), log(fH_2O/fHF), and log($fHF/fHCl$) ratios of magmatic fluids in equilibrium with magmas are shown in Fig. 7. The log($fHF/fHCl$) increases gradually from Group I (−1.94 to -0.58, ave. −1.19), through Group II (−0.64 to -0.43, ave. −0.57) and Group III (−1.06 to -0.31, ave. −0.47), to Donggou porphyry (−0.05 to 0.17, ave. 0.07), whereas the log(fH_2O/fHF) decreases from Group I (4.51–5.45, ave. 4.94), through Group II (4.16–4.24, ave. 4.20) and Group III (3.86–4.61, ave. 4.06), to Donggou porphyry (3.79–3.81, ave. 3.80). The log($fH_2O/fHCl$) ranges from 3.48 to 4.04, with the highest values in the biotites from the Donggou porphyry.

8. Discussion

8.1. The relationship between the Taishanmiao batholith and Donggou porphyry

It has long been controversial whether the Donggou porphyry is genetically related to the slightly older Taishanmiao batholiths (Ye et al., 2006; Dai et al., 2009; Huang et al., 2009).

The decrease in K/Rb ratios in biotite has previously been regarded as an index of magmatic differentiation (Zhang et al., 2016). As mentioned above, the K/Rb ratios, compatible elements (Co, Ba, V and Ti) and incompatible elements (Cs, Li, Ta and Tl) of biotite decrease or increase gradually from the coarse-grained syenogranite (Group I), through the medium-graind syenogranite (Group II), to the porphyritic syenogranite (Group III) and the Donggou porphyry. These geochemical characteristics indicate a magma evolution trend from Group I rocks, through Group II, to Group III and the Donggou porphyry (Fig. 5). The result is also proved by the major and trace-element data of the whole rocks, with decreasing TiO_2, FeO^*, MgO, P_2O_5, Ba and V, and increasing Mo, Rb and SiO_2 from Group I, through Group II and Group III, to Donggou porphyry (Ye et al., 2008; and our unpublished data). In addition, the $\varepsilon_{Nd}(t)$ and $\varepsilon_{Hf}(t)$ of the Donggou porphry are −13.2 to −17.3 and −3.4 to −19.9, respectively, similar to those of the Taishanmiao batholith (Dai et al., 2009; Yang et al., 2013a; Gao et al., 2014b; Wang et al., 2016).

It is notable that the zircon U-Pb ages of the Taishanmiao batholith and Donggou porphyry vary from 125 to 120 Ma and 118 to 117 Ma, respectively (Gao et al., 2014b; Qi, 2014; Wang et al., 2016; Yang et al., 2013a). The age of the Donggou porphyry is about ca. 3 Ma later than that of the Group III of the Taishanmiao batholith. Many geochronological studies of volcanic and plutonic rocks suggest that magmatic system may be long-lived, on the order of $> 10^5$ to $> 10^6$ years (Walker et al., 2007 and reference therein). Brown and Mcclelland (2000) suggested the crystallization periods can last as much as 8 Ma for individual batholiths, a likely consequence of construction by episodic pulses of magma. In addition, the geophysical data indicate that the Taishanmiao batholith is connected with the Donggou porphyry in deep level (Ye et al., 2006). Thus, we consider that the Donggou porphyry is a branch of the Taishanmiao batholith.

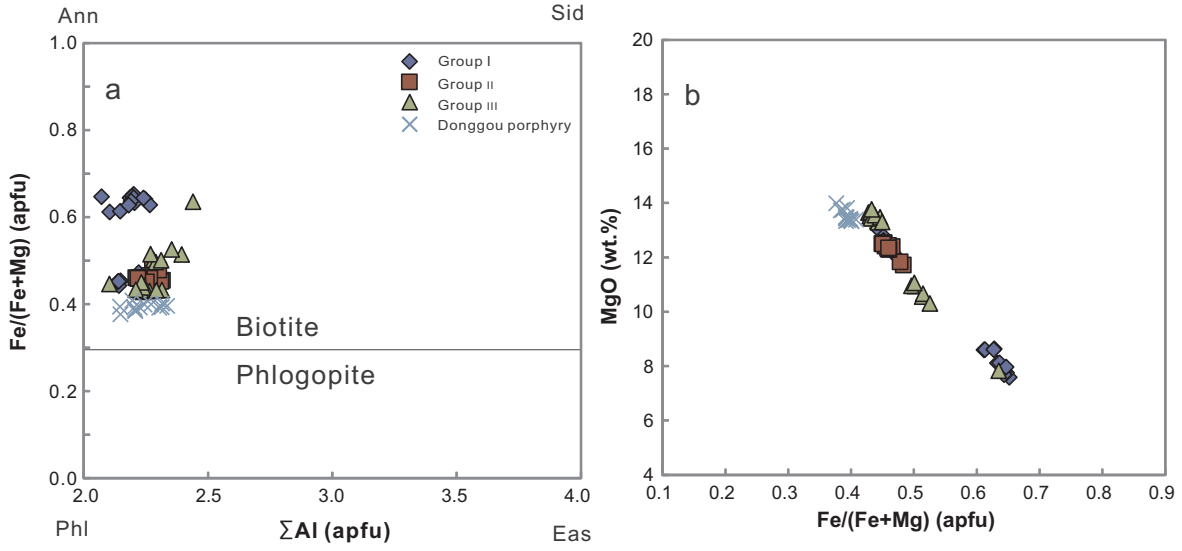

Fig. 4. Chemical compositional diagrams of biotite from the Taishanmiao batholith and Donggou porphyry. (a) Fe/(Fe + Mg) − ΣAl (apfu) (apfu = atoms per formula unit) diagram after Rieder et al. (1998), (b) diagram of MgO (wt%) vs. Fe/(Fe + Mg) (apfu).

In summary, both geochemical and geochronological data suggest that the Donggou porphyry is a highly differentiated product of the Taishanmiao batholith.

8.2. Metallogenic implication

8.2.1. Variations of oxygen fugacity and metal concentrations during magmatic differentiation

The link between the oxidation state of granitoids and metallic mineralization is well-known (Candela, 1992; Hedenquist and Lowenstern, 1994; Ballard et al., 2002; Mungall, 2002). Formation of Mo porphyries or Mo-bearing granites are usually associated with oxidized magmas (Blevin and Chappell, 1992; Li et al., 2012c; Sun et al., 2015), whereas W-Sn deposits are related to reduced magmas (Lehmann and Mahawat, 1989; Lehmann, 1990; Blevin and Chappell, 1992; Mengason et al., 2011).

The compositions of biotite from the Taishanmiao batholith and Donggou porphyry are plotted mostly above the nickel-nickel oxide

Table 2
Average contents of trace elements in biotite from the felsic intrusive rocks around the Donggou Porphyry Mo deposit analyzed by laser ablation-inductively coupled plasma-mass spectrometry (LA-ICP-MS).

	Group I			Group II			Group III			Donggou granite porphyry		
	ave.	Int2SE	LOD	ave.	Int2SE	LOD	ave.	Int2SE	LOD	ave.	Int2SE	LOD
wt%												
TiO_2	3.70	0.10	7.66E-04	3.49	0.17	4.37E-04	2.35	0.06	2.90E-04	2.19	0.06	2.94E-04
Al_2O_3	12.4	0.22	1.49E-04	13.1	0.26	1.84E-04	12.8	0.23	2.14E-04	12.91	0.57	3.09E-04
FeO	22.9	0.87	8.99E-03	19.1	1.28	5.91E-03	19.1	0.68	4.51E-03	15.75	0.66	4.89E-03
MnO	0.68	0.03	2.48E-04	0.67	0.06	2.84E-04	0.68	0.03	2.30E-04	1.31	0.02	2.58E-04
MgO	9.77	0.31	1.99E-04	12.4	0.54	3.30E-04	12.7	0.31	3.53E-04	13.79	0.21	4.64E-04
CaO	0.01	0.01	6.25E-02	0.02	0.03	6.87E-02	0.01	0.01	5.74E-02	0.05	0.02	6.12E-02
NaO	0.20	0.01	2.12E-03	0.20	0.02	2.56E-03	0.17	0.01	2.22E-03	0.14	0.00	3.01E-03
K_2O	9.37	0.40	1.48E-03	8.82	0.55	1.67E-03	8.57	0.31	1.36E-03	9.11	0.22	2.24E-03
ppm												
Li	496	19.8	1.84	696	55.3	1.78	1084	37.9	1.56	1548	16.8	1.96
Sc	20.8	0.68	0.87	43.5	1.87	0.84	41.6	1.23	0.57	69.2	2.08	0.91
V	81.6	2.65	0.31	55.3	3.76	0.21	10.4	0.82	0.15	15.7	2.08	0.18
Cr	6.99	1.95	6.39	26.4	5.07	9.17	14.1	2.00	8.30	133	18.2	7.63
Co	41.7	1.69	0.08	38.1	2.25	0.05	26.5	0.96	0.05	18.6	0.70	0.06
Ni	5.14	0.55	1.58	20.2	1.63	1.01	4.35	0.42	0.97	9.67	0.81	1.12
Zn	762	32.1	6.27	550	36.4	4.25	519	23.0	3.20	1178	49.2	3.70
Ga	66.9	2.87	0.19	59.6	3.40	0.19	60.2	2.29	0.15	118	4.19	0.19
Rb	762	31.1	0.13	868	52.4	0.14	1347	68.2	0.08	1657	38.7	0.21
Nb	136	4.70	0.02	157	9.00	0.00	198	7.02	0.00	326	24.4	0.00
Mo	0.64	0.12	0.04	1.20	0.23	0.05	1.33	0.20	0.00	8.26	0.92	0.02
Sn	5.60	0.42	1.71	9.90	1.00	1.49	22.3	0.94	1.50	22.2	0.91	1.82
Cs	6.37	0.44	0.02	5.05	0.35	0.04	17.8	1.72	0.05	55.4	1.81	0.09
Ba	3863	63.7	0.30	845	35.2	0.08	137	3.57	0.08	44.0	7.66	0.07
Ta	2.51	0.13	0.06	2.43	0.21	0.01	12.5	0.42	0.00	31.8	1.53	0.01
W	0.21	0.07	0.08	0.28	0.09	0.10	0.48	0.09	0.06	1.05	7.02	0.02
Tl	3.83	0.24	0.09	3.23	0.33	0.09	6.77	0.33	0.07	18.8	0.38	0.06
Pb	6.38	0.40	0.42	6.66	0.73	0.37	7.08	0.84	0.32	51.5	7.11	0.40

Note: SiO_2 content for each spot measured by EMPA is used for internal standardization. Int2SE is the analytical error. LOD is the limit of detection which is shown in wt% and ppm for the major and trace elements, respectively.

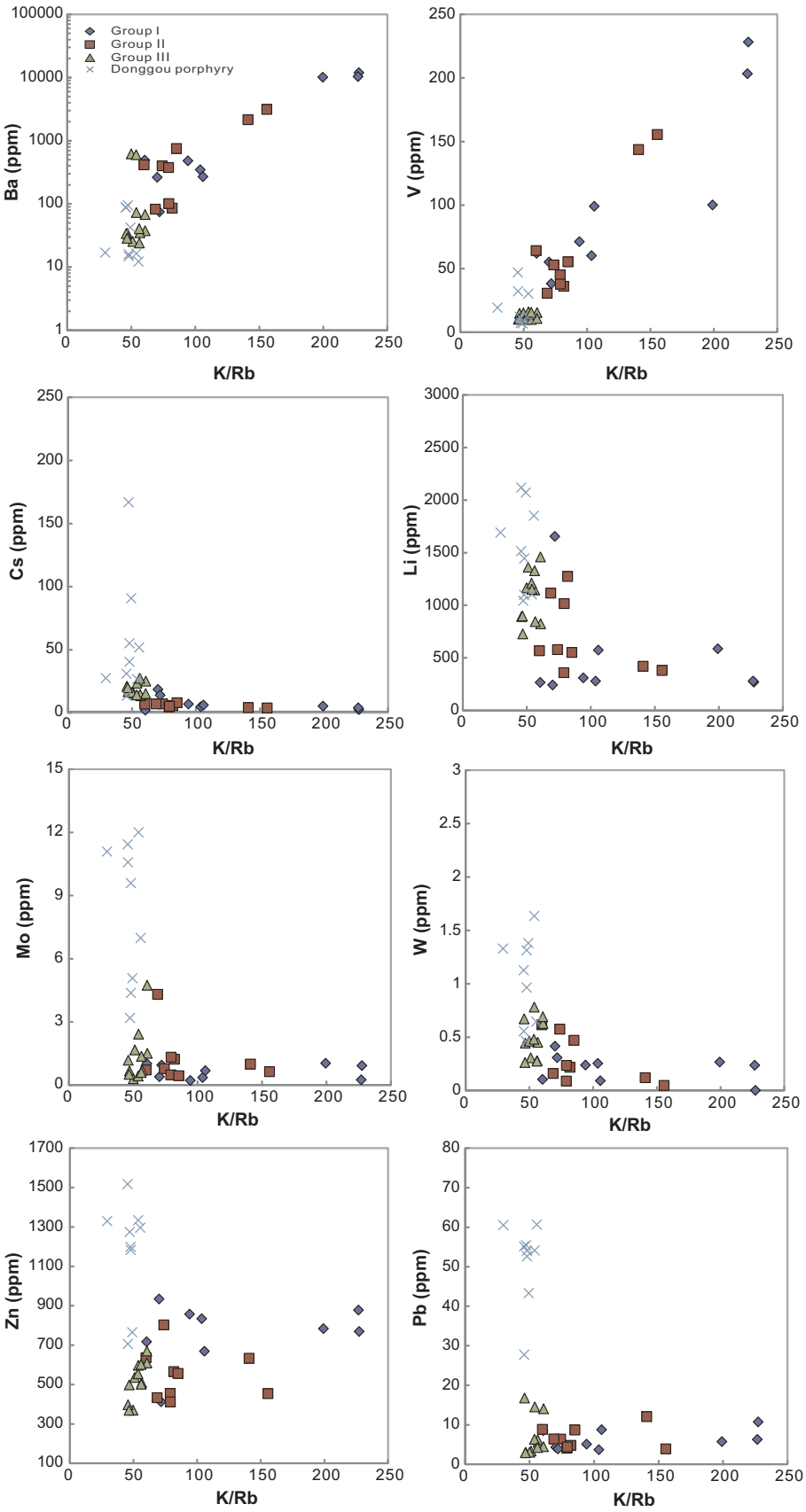

Fig. 5. Trace-element compositions of biotite from the Taishanmiao batholith and Donggou porphyry analyzed by LA-ICP-MS.

(NNO) buffer in the Fe^{2+}-Fe^{3+}-Mg diagram of Wones and Eugster (1965), indicating that these granitoids formed at relatively high oxygen fugacity (Fig. 8). In addition, the presence of the assemblage of titanite + magnetite + quartz, which is indicative of oxygen fugacities above ~QFM + 1 log unit at 800 °C (Piccoli et al., 2000), is also consistent with a relatively high oxygen fugacity. It is noteworthy that the

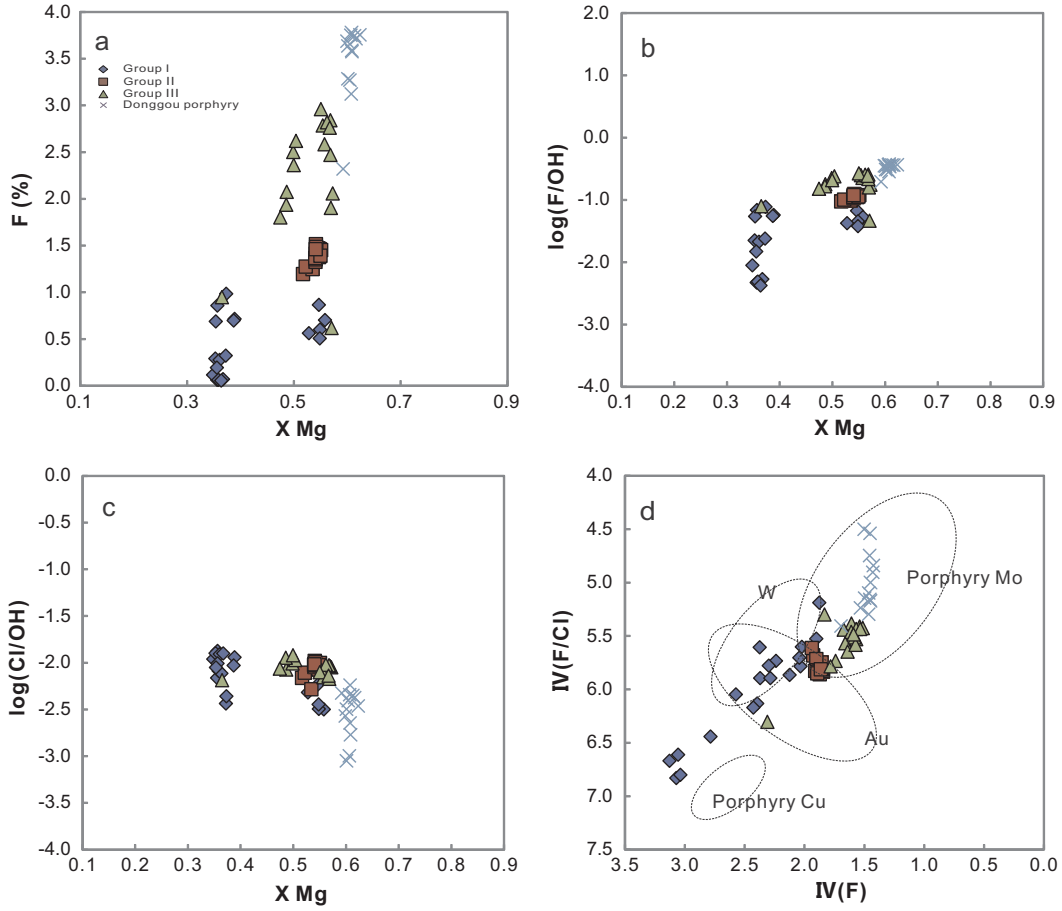

Fig. 6. Compositions of biotite from the Taishanmiao batholith and Donggou porphyry on (a) F (wt%) vs. X_{Mg} for biotites, while X_{Mg} is the ratio of Mg/(Mg + Fe) (apfu). (b), (c) X_{Mg} vs $\log(X_F/X_{OH})$ and $\log(X_{Cl}/X_{OH})$. (d) intercept value IV(F/Cl) vs IV(F). See text for explanation.

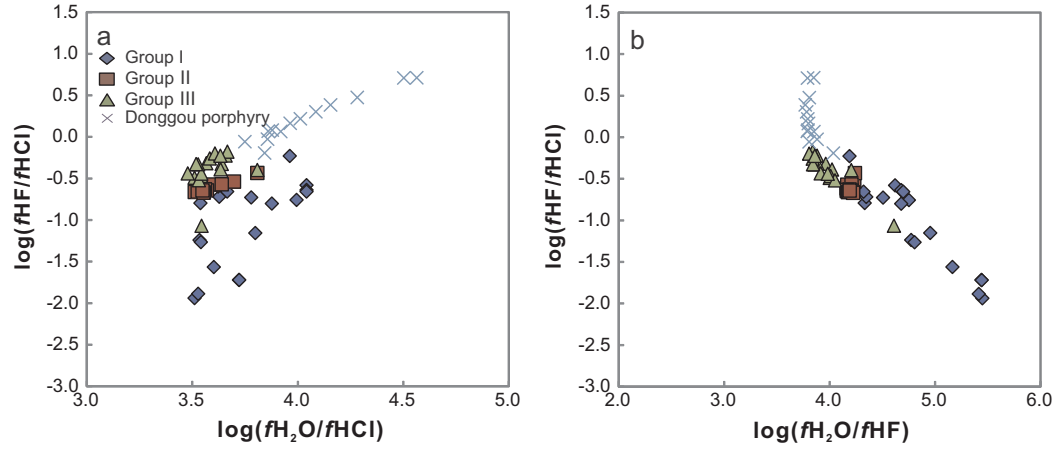

Fig. 7. Correlations of $\log(fH_2O/fHCl)$, $\log(fH_2O/fHF)$, and $\log(fHF/fHCl)$ values in fluids in equilibrium with biotite from the Taishanmiao batholith and the Donggou porphyry. These values were calculated based on their relative zircon saturation temperatures (T_{Zr}) (Watson and Harrison, 1983).

Fe^{3+}/Fe^{2+} values of biotite gradually increase from Group I (ave. 0.19), through Group II (ave. 0.30) and Group III (ave. 0.28), to the Donggou porphyry (ave. 0.37), indicating progressive increasing fO_2 during magmatic differentiation, which may be attributed to H_2 release at or near H_2O vapor saturation at high H_2O/Fe^{2+} (Candela, 1986a; Lentz, 1992).

Oxidation state of magmas controls sulfur speciation and hence strongly influences sulfur solubility of the magmas (Jugo, 2009; Yang, 2012). Some scholars consider that the early crystallization and separation of sulfides from magma may cause Mo depletion in residual melt (Mengason et al., 2011; Qiu et al., 2013). Experiments of Mengason et al. (2011) indicate that the $D_{Mo}^{sulfide/silicate\ melt}$ is 35 at the NNO oxygen fugacity buffer and increases with decreasing oxygen fugacity. It is thus suggested that highly evolved, oxidized felsic melts (magmatic oxygen fugacity > NNO, magnetite-series granites) may have lost as much as 14% of their initial molybdenum, whereas reduced melts (magmatic oxygen fugacity < NNO-0.5, ilmenite-series granites) may have lost 90% of the initial molybdenum. However, the solubility of sulfur in felsic magmas is very low (< 1000 ppm) (Clemente et al., 2004; Yang, 2012). Even if a large proportion of the sulfides

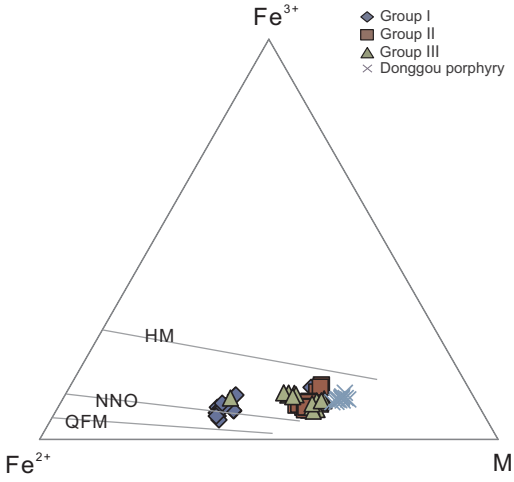

Fig. 8. Compositions of biotite from the Taishanmiao batholith and Donggou porphyry expressed in the Fe^{2+}-Fe^{3+}-Mg diagram of Wones and Eugster (1965), along with the three common $f(O_2)$ (oxygen fugacity) buffers: quartz-fayalite-magnetite (QFM), nickel-nickel oxide (NNO), and hematite-magnetite (HM). The Fe^{3+} in biotite is calculated according to Dymek (1983).

(pyrrhotite) is separated from the magma, it would not cause Mo depletion in the residual melt. Therefore, we consider that sulfides removal in felsic magma is very limited under high or low oxygen fugacity.

Oxygen fugacity can influence the valence of molybdenum in magma. Mo^{6+} may be the predominant phase in magmas at oxygen fugacity buffer of NNO or above, and thus would not substitute Ti in the crystallizing Fe- and Ti-rich minerals (Candela and Holland, 1986; Tacker and Candela, 1987). In our case, the oxygen fugacity is remarkably high and gradually increases during magmatic differentiation (Fig. 8), and hence enhances the incompatibility of Mo (Tacker and Candela, 1987; Candela and Bouton, 1990). Thus, Mo concentrations in granitoids also gradually increase from Group I (ave. 0.96 ppm), through II (ave. 0.98 ppm) and III (ave. 1.12 ppm), to the Donggou porphyry (ave. 18.72 ppm) (Ye et al., 2008; Dai et al., 2009 and our unpublished data). As such, Mo was initially concentrated during magma crystallization, and thus the exsolved hydrothermal fluids from this oxidized and differentiated magma would contain elevated Mo contents.

8.2.2. Implications for halogen elements in the magmas

As volatiles can play an important effect on melt properties and magma evolution, it is important to know the actual contents of volatiles in the melt. According to the experimental result of Icenhower and London (1997), the partitioning of fluorine and chlorine between biotite and melt has an approximate linear relationship with Mg‘ [100 Mg/(Mg + Mn + Fe)]. Based on this relationship, the contents of fluorine and chlorine in melt were calculated to be 0.02–0.78% and 0.02–0.07%, respectively. It is clear that the melts are rich in fluorine with the highest fluorine concentration in the Donggou porphyry (Fig. 6a). Given that water saturation was reached during crystallization, chlorine is strongly partitioned into fluid over melt when an magmatic volatile phase (MVP) was exsolved. In contrast, fluorine will act an opposite behavior, and will consistently partition into minerals relative to melt (Zhu and Sverjensky, 1991). Thus, the Cl/F and OH/F of the melts will decrease with magma differentiation (Fig. 6) once volatiles were released from the magma system (Candela, 1986b; Keith et al., 1989; van Middelaar and Keith, 1990; Loferski and Ayuso, 1995; Christiansen and Keith, 1996; Webster, 1997a,b).

Moreover, the experimental results of Nash and Crecraft (1985) indicate that the partition coefficient of molybdenum between biotite and rhyolite varies from 1.7 to 5.7. Based on the minimum partition coefficient of 1.7, we calculated the Mo contents of the Donggou porphyric magma ranging from 1.87 to 7.06 ppm, consistent with Mo concentrations in melt inclusions associated with many porphyry Mo systems (2–20 ppm; Lowenstern, 1994; Audétat, 2010, 2015; Audétat et al., 2011; Mercer et al., 2015). Such low concents of Mo indicate that the Donggou porphyry covering an area of only ~0.01 km^2, cannot be the sole Mo source for the giant Donggou Mo deposit. Lowenstern (1994) and Shinohara et al. (1995) proposed that the formation of porphyry Mo deposits results from the circulation of volatile-rich magma within narrow stocks or apophyses protruding from underling batholith of metal magma chambers, and the formation of stocks or apophyses requires efficient segregation of fractionated melts at the top of the magma chamber. Indeed, the F enrichment in the Donggou porphyry can promote high degrees of melt fractionation by lowering the magma solidus to extend the crystallization interval, and by lowering the melt viscosity to facilitate residual melt extraction and accumulation in the apical regions of magma chambers (Audétat, 2015). The high degrees of melt fractionation would promote the enrichment of molybdenum in the residual magma of which the circulation was responsible for the formation of the superlarge Donggou porphyry Mo deposit.

In addition, the log(fHF/fHCl) ratio of earlier fluids derived from the Taishanmiao batholith is less than 0, whereas the log(fHF/fHCl) ratio of later fluids derived from the Donggou porphyry is more than 0 (Fig. 7). Cline and Bodnar (1991) showed the salinity of the exsolving fluid increases as crystallization proceeds at pressures below 1.3 kbar, whereas at pressures slightly greater than 1.3 kbar, the salinity of exsolving fluids gradually decreases. According to the study of Yang et al. (2015), the ore-forming pressures were estimated to be less than 1.3 kbar in the earliest mineralization stage in the Donggou Mo deposit. Therefore, we consider that the salinity of exsolving fluid may gradually increase or stay constant from the Taishanmiao batholith to Donggou porphyry. Thus the earlier fluids associated with the Taishanmiao batholith are relatively F-poor, whereas the later fluids associated with the Donggou porphyry are relatively F-rich. Though the majority of dissolved molybdenum species in hydrothermal solutions occur as H_2MoO_4, $HMoO_4^-$, and MoO_4^{2-} (Shock et al., 1997; Rempel et al., 2009), the fluorine in fluids may also have important effects on partitioning Mo between melt and fluid and transporting Mo (Carten et al., 1981; Candela and Holland, 1984; Keppler and Wyllie, 1991; Bai and van Groos, 1999). The $D_{Mo}^{fluid/melt}$ was higher in the fluorine-containing system than in the presence of chloride in previous experiments (Candela and Holland, 1984; Keppler and Wyllie, 1991; Bai and van Groos, 1999). Therefore, the transition of the fluid compositions from relatively F-poor in the Taishanmiao batholith to relatively F-rich in the Donggou porphyry may be beneficial to concentrate Mo in the fluids associated with the Donggou porphyry.

8.3. Comparison of halogen fugacity ratios with porphyry Cu deposits

To better understand the physicochemical conditions of the magmatic fluids, halogen fugacity ratios of biotites from the Taishanmiao batholith and the Donggou porphyry are compared with those of fluids associated with porphyry Mo-/Cu-related plutons worldwide (Fig. 9).

Magmatic fluids associated with the Donggou porphyry have log ($f$$H_2O$/$f$HCl) and log ($f$HF/$f$HCl) values similar to or slightly higher than those for Climax, Henderson, Yuchling, Nannihu and Leimengou porphyry Mo deposits, but significantly higher than those for porphyry Cu and Cu-Mo deposits (Fig. 9a). Moreover, the magmatic fluids associated with the Donggou porphyry have similar or slightly lower log ($f$$H_2O$/$f$HF) values compare to those for other porphyry Mo deposits, but much lower than those for porphyry Cu and Cu-Mo deposits (Fig. 9b). Because the compositions of biotite in porphyry Cu-Mo deposits are limited in published literatures, we just calculate the halogen fugacity ratios in one deposit (Luoboling). Interestingly, the Luoboling porphyry Cu-Mo deposit has similar halogen fugacity ratios to other porphyry Cu

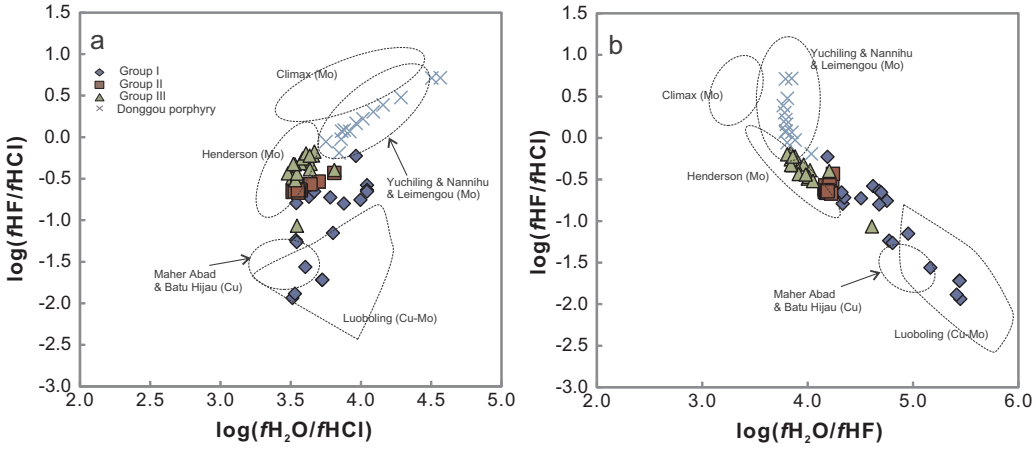

Fig. 9. The calculated halogen fugacity ratios of fluids in equilibrium with biotite from the Taishanmiao batholith and Donggou porphyry in comparison to those of other porphyry Mo deposits (Henderson, Climax, Yuchiling, Nannihu and Leimengou), porphyry Cu-Mo deposit (Luoboling) and porphyry Cu deposits (Maher Abad and Batu Hijau); (a) log ($fH_2O/fHCl$) against log ($fHF/fHCl$) and (b) log (fH_2O/fHF) against log ($fHF/fHCl$). The recalculated fugacity ratios are determined from the compositions of biotite in the Mo-related granitoids in Climax (Audétat, 2015) and Henderson (Mercer et al., 2015) in North America, and in Yuchiling, Nannihu and Leimengou (our unpublished data) at the southern margin of the North China Craton, as well as in the porphyry Cu-related plutons in the Maher Abad (Siahcheshm et al., 2012) in eastern Iran, and Batu Hijau (Idrus et al., 2007) in Indonesia and in the porphyry Cu-Mo-related plutons in the Luoboling (Li and Jiang, 2015) in south China based on the equations of Munoz (1992), and temperatures established from mineral or mineral pair geothermometry, e.g., 720 °C for Climax, 612–768 °C for Henderson, 758 °C for Maher Abad, 764 °C for Batu Hijau and 750 °C for Luoboling.

deposits, not situated between the porphyry Mo and Cu deposits. In fact, the size of Mo ore body is very small in this deposit, with proven reserves of 0.065 Mt Mo (metal) with an average grade of 0.036% (Li and Jiang, 2015). Therefore, we consider that these similar characteristics between Luoboling Cu-Mo and other Cu deposits may explain why the dominated Cu mineralization is formed in Luoboling.

According to the study of Audétat et al. (2008), the fluids exsolving from porphyry Mo and porphyry Cu systems appear to be similar in terms of fluid salinity. Therefore, the magmatic fluids related to porphyry Mo deposits are characterized by higher fluorine contents relative to those from porphyry Cu deposits. The difference between porphyry Mo deposits and porphyry Cu deposits may depend on the source of magma. Formation of porphyry Cu deposits are commonly related to subduction of oceanic crust that is generally Cl-rich (Sillitoe, 2010), whereas that of porphyry Mo deposits are related to continental crust that is F-rich (Sinclair, 2007; Chen and Li, 2009; Hou and Yang, 2009; Zhu et al., 2009). In addition, experimental studies indicate the Cl-rich fluids are more beneficial to extract Cu from the melt and transport copper (Candela and Holland, 1984; Keppler and Wyllie, 1991; Bai and van Groos, 1999). The above results indicate that the relatively F-rich fluids may be favorable to form porphyry Mo deposits.

9. Conclusions

The Donggou porphyry is interpreted to be the product of highly differentiation of the Taishanmiao batholith. Variations of the K/Rb ratio, compatible elements (such as Co, Ba, V and Ti) and imcompatible elements (such as Cs, Li, Ta and Tl) of biotite in these granitoids were controlled by magma differentiation.

Fe^{3+}/Fe^{2+} and MgO values in biotite gradually increase from the Taishanmiao batholith to the Donggou porphyry, which indicates progressively increasing fO_2 during magmatic differentiation. The majority of biotite compositions indicate high oxygen fugacity above the NNO buffer, indicative of Mo^{6+} as the predominant valence in the magma. In such a condition, Mo acted as an incompatible element and concentrated in the residual melt.

Metals were further concentrated into the fluids that were exsolved from magma. The earlier fluids associated with the Taishanmiao batholith are relatively F-poor, whereas the later fluids associated with the Donggou porphyry are relatively F-rich. We propose that the relatively F-rich fluids from the Donggou porphyry may be beneficial to form the porphyry Mo deposit.

Acknowledgements

This research was supported by the fund from the National Key Research and Development Program of China (grant number 2016YFC0600106), the National Natural Science Foundation of China (grant number 41373046) and the "Thousand Youth Talents Plan" grant to Wei Terry Chen. We highly appreciate Prof. Zhi-Wei Bao, Alexandra Yang Yang and Dr. Xiaochun Li for their helpful suggestions and language improvement on drafts of the manuscript. We also appreciate the Jinduicheng Molybdenum Group Co., Ltd. for the field work in the Donggou Mine. Many thanks go out to Professor Franco Pirajno, Dr. Yanbo Cheng, Andreas Audétat and two anonymous referees for their constructive comments that helped improve substantially the manuscript.

Appendix A. Supplementary data

Supplementary data associated with this article can be found, in the online version, at http://dx.doi.org/10.1016/j.oregeorev.2017.10.026.

References

Abdel-Rahman, A.F.M., 1994. Nature of biotites from alkaline, calc-alkaline, and peraluminous magmas. J. Petrol. 35, 525–541.
Audétat, A., 2010. Source and evolution of molybdenum in the porphyry Mo(-Nb) deposit at cave peak, Texas. J. Petrol. 51, 1739–1760.
Audétat, A., 2015. Compositional evolution and formation conditions of magmas and fluids related to porphyry mo mineralization at climax. Colorado. J. Petrol. 56, 1519–1546.
Audétat, A., Pettke, T., Heinrich, C.A., Bodnar, R.J., 2008. Special paper: the composition of magmatic-hydrothermal fluids in barren and mineralized intrusions. Econ. Geol. 103, 877–908.
Audétat, A., Dolejš, D., Lowenstern, J.B., 2011. Molybdenite saturation in silicic magmas: occurrence and petrological implications. J. Petrol. 52, 891–904.
Ayati, F., Yavuz, F., Noghreyan, M., Haroni, H.A., Yavuz, R., 2008. Chemical characteristics and composition of hydrothermal biotite from the Dalli porphyry copper prospect, Arak, central province of Iran. Mineral. Petrol. 94, 107–122.
Bai, T.B., van Groos, A.F.K., 1999. The distribution of Na, K, Rb, Sr, Al, Ge, Cu, W, Mo, La, and Ce between granitic melts and coexisting aqueous fluids. Geochim. Cosmochim. Acta 63, 1117–1131.
Ballard, J.R., Palin, M.J., Campbell, I.H., 2002. Relative oxidation states of magmas inferred from Ce(IV)/Ce(III) in zircon: application to porphyry copper deposits of northern Chile. Contrib. Mineral. Petrol. 144, 347–364.
Bao, Z.W., Wang, C.Y., Zhao, T.P., Li, C.J., Gao, X.Y., 2014. Petrogenesis of the Mesozoic granites and Mo mineralization of the Luanchuan ore field in the East Qinling Mo mineralization belt, Central China. Ore Geol. Rev. 57, 132–153.
Blevin, P.L., Chappell, B.W., 1992. The role of magma sources, oxidation states and fractionation in determining the granite metallogeny of eastern Australia. Trans. R. Soc. Edinburgh Earth Sci. 83, 305–316.
Brown, E.H., Mcclelland, W.C., 2000. Pluton emplacement by sheeting and vertical ballooning in part of the southeast Coast Plutonic Complex, British Columbia. Geol. Soc. Am. Bull. 112, 708–719.

Candela, P.A., 1986a. The evolution of aqueous vapor from silicate melts: effect on oxygen fugacity. Geochim. Cosmochim. Acta 50, 1205–1211.
Candela, P.A., 1986b. Toward a thermodynamic model for the halogens in magmatic systems: an application to melt-vapor-apatite equilibria. Chem. Geol. 57, 289–301.
Candela, P.A., 1992. Controls on ore metal ratios in granite-related ore systems: an experimental and computational approach. Geol. Soc. Am. Spec. Pap. 272, 317–326.
Candela, P.A., Bouton, S.L., 1990. The influence of oxygen fugacity on tungsten and molybdenum partitioning between silicate melts and ilmenite. Econ. Geol. 85, 633–640.
Candela, P.A., Holland, H.D., 1984. The partitioning of copper and molybdenum between silicate melts and aqueous fluids. Geochim. Cosmochim. Acta 48, 373–380.
Candela, P.A., Holland, H.D., 1986. A mass transfer model for copper and molybdenum in magmatic hydrothermal systems; the origin of porphyry-type ore deposits. Econ. Geol. 81, 1–19.
Carten, R.B., Shannon, J.R., Ward, A.D., Geraghty, E.P., 1981. Controls on molybdenite deposition at Henderson Mine, Empire, Colorado. Geol. Soc. Am. 13, 423 Abstracts with Programs.
Chen, Y.J., Li, N., 2009. Nature of ore-fluids of intracontinental intrusion-related hydrothermal deposits and its difference from those in island arcs. Acta Petrol. Sin. 25, 2477–2508 (in Chinese with English abstract).
Chen, Y.J., Pirajno, F., Li, N., Guo, D.S., Lai, Y., 2009. Isotope systematics and fluid inclusion studies of the Qiyugou breccia pipe-hosted gold deposit, Qinling Orogen, Henan province, China: implications for ore genesis. Ore Geol. Rev. 35, 245–261.
Chen, X., Ye, H., Wang, H., 2014. Genesis and evolution of the Leimengou porphyry Mo deposit in WestHenanProvince, East Qinling-Dabie belt, China: constraints from hydrothermal alteration, fluid inclusions and stable isotope data. J. Asian Earth Sci. 79, 710–722.
Christiansen, E.H., Keith, J.D., 1996. Trace element systematics in silicic magmas: a metallogenic perspective. In: Wyman, D.A. (Ed.), Trace Element Geochemistry of Volcanic Rocks: Applications for Massive Sulphide Exploration. Geological Association of Canada, Short Course Notes 12, pp. 115–151.
Clemente, B., Scaillet, B., Pichavant, M., 2004. The solubility of sulphur in hydrous rhyolitic melts. J. Petrol. 45, 2171–2196.
Cline, J.S., Bodnar, R.J., 1991. Can economic porphyry copper mineralization be generated by a typical calc-alkaline melt? J. Geophys. Res. 96, 8113–8126.
Coulson, I.M., Dipple, G.M., Raudsepp, M., 2001. Evolution of HF and HCl activity in magmatic volatiles of the gold-mineralized EmeraldLake pluton, Yukon Territory, Canada. Mineral. Deposita 36, 594–606.
Dai, B.Z., Jiang, S.Y., Wang, X.L., 2009. Petrogenesis of the granitic porphyry related to the giant molybdenum deposit in Donggou, Henan province, China: constraints from petrogeochemistry, zircon U-Pb chronology and Sr-Nd-Hf isotopes. Acta Petrol. Sin. 25, 2889–2901 (in Chinese with English abstract).
Dingwell, D.B., 1989. Effect of fluorine on the viscosity of diopside liquid. Am. Mineral. 74, 333–338.
Dymek, R.F., 1983. Titanium, aluminum and interlayer cation substitutions in biotite from high-grade gneisses, West Greenland. Am. Mineral. 68, 880–899.
Fu, Z.G., Song, Y.W., Lu, Y.H., 2006. Ore-controlling geology condition and prospecting information of Donggou Mo deposit in Ruyang, Henan Province. Geophys. Prospect. 42, 33–38 (in Chinese with English abstract).
Gao, X.Y., Zhao, T.P., Yuan, Z.L., Zhou, Y.Y., Gao, J.F., 2010. Geochemistry and petrogenesis of the Heyu batholith in southern margin of the North China Block. Acta Petrol. Sin. 26, 3485–3506 (in Chinese with English abstract).
Gao, Y., Ye, H., Mao, J., Li, Y., 2013. Geology, geochemistry and genesis of the Qianfanling quartz-vein Mo deposit in SongxianCounty, Western Henan Province, China. Ore Geol. Rev. 55, 13–28.
Gao, X.Y., Zhao, T.P., Chen, W.T., 2014a. Petrogenesis of the early Cretaceous Funiushan granites on the southern margin of the North China Craton: implications for the Mesozoic geological evolution. J. Asian Earth Sci. 94, 28–44.
Gao, X.Y., Zhao, T.P., Bao, Z.W., Yang, A.Y., 2014b. Petrogenesis of the early Cretaceous intermediate and felsic intrusions at the southern margin of the North China Craton: implications for crust–mantle interaction. Lithos 206–207, 65–78.
Gao, Y., Mao, J., Ye, H., Meng, F., Li, Y., 2015. A review of the geological characteristics and geodynamic setting of the late Early Cretaceous molybdenum deposits in the East Qinling-Dabie molybdenum belt, East China. J. Asian Earth Sci. 108, 81–96.
Grabezkev, A.I., Vigorova, V.G., Chashukhina, V.A., 1979. Behavior of fluorine during crystallization of granites (in connection with validation of the criteria of granite specialization). Geochem. Int. 16, 23–33.
Gunow, A.J., Ludington, S., Munoz, J.L., 1980. Fluorine in micas from the Henderson molybdenite deposit, Colorado. Econ. Geol. 75, 1127–1137.
Han, Y.G., Zhang, S.H., Pirajno, F., Zhou, X.W., Zhao, G.C., Qü, W.J., Liu, S.H., Zhang, J.M., Liang, H.B., Yang, K., 2013. U-Pb and Re–Os isotopic systematics and zircon Ce4+/Ce3+ ratios in the Shiyaogou Mo deposit in eastern Qinling, central China: insights into the oxidation state of granitoids and Mo (Au) mineralization. Ore Geol. Rev. 55, 29–47.
Hedenquist, J.W., Lowenstern, J.B., 1994. The role of magmas in the formation of hydrothermal ore deposits. Nature 370, 519–527.
Hou, Z.Q., Yang, X.M., 2009. Porphyry deposits in continental settings of China : geological characteristics, magmatic-hydrothermal system, and metallogenic model. Acta Geol. Sinica 83, 1779–1817 (in Chinese with English abstract).
Huang, F., Luo, Z.H., Lu, X.X., Gao, F., Chen, B.H., Yang, Z.F., Pan, Y., Li, D.D., 2009. Was Donggou porphyry Mo deposit derived from Taishanmiao batholiths? Miner. Deposits 28, 569–584 (in Chinese with English abstract).
Icenhower, J.P., London, D., 1997. Partitioning of fluorine and chlorine between biotite and granitic melt: experimental calibration at 200 MPa H 2 O. Contrib. Mineral. Petrol. 127, 17–29.
Idrus, A., Kolb, J., Meyer, F.M., 2007. Chemical composition of rock-forming minerals in copper? Gold-bearing tonalite porphyries at the Batu Hijau deposit, Sumbawa Island, Indonesia: implications for crystallization conditions and fluorine? Chlorine fugacity. Resour. Geol. 57, 102–113.
Jugo, P.J., 2009. Sulfur content at sulfide saturation in oxidized magmas. Geology 37, 415–418.
Keith, J.D., van Middelaar, W., Clark, A.H., Hodgson, C.J., 1989. Granitoid textures, compositions, and volatile fugacities associated with the formation of tungsten-dominated skarn deposits. In: Whitney, J.A., Naldrett, A.J. (Eds.), Ore Deposition Associated with Magmas. Rev. Econ. Geol., vol. 4. pp. 235–250.
Keppler, H., 1993. Influence of fluorine on the enrichment of high field strength trace elements in granitic rocks. Contrib. Mineral. Petrol. 114, 479–488.
Keppler, H., Wyllie, P.J., 1991. Partitioning of Cu, Sn, Mo, W, U, and Th between melt and aqueous fluid in the systems haplogranite-H2O − HCl and haplogranite-H2O − HF. Contrib. Mineral. Petrol. 109, 139–150.
Kröner, A., Compston, W., Zhang, G.W., Guo, A.L., Todt, W., 1988. Age and tectonic setting of Late Archean greenstone-gneiss terrain in Henan Province, China, as revealed by single-grain zircon dating. Geology 16, 211–215.
Lehmann, B., 1990. Large-scale tin depletion in the Tanjungpandan tin granite, Belitung Island, Indonesia. Econ. Geol. 85, 99–111.
Lehmann, B., Mahawat, C., 1989. Metallogeny of tin in central Thailand: a genetic concept. Geology 17, 426–429.
Lentz, D., 1992. Petrogenesis and geochemical composition of biotites in rare-element granitic pegmatites in the Southwestern Grenville Province, Canada. Mineral. Petrol. 46, 239–256.
Li, B., Jiang, S.Y., 2015. A subduction-related metasomatically enriched mantle origin for the Luoboling and Zhongliao Cretaceous granitoids from South China: implications for magma evolution and Cu–Mo mineralization. Int. Geol. Rev. 57, 1239–1266.
Li, X., Zhou, M.F., 2015. Multiple stages of hydrothermal REE remobilization recorded in fluorapatite in the Paleoproterozoic Yinachang Fe–Cu–(REE) deposit, Southwest China. Geochim. Cosmochim. Acta 166, 53–73.
Li, N., Chen, Y.J., Zhang, H., Zhao, T.P., Deng, X.H., Wang, Y., Ni, Z.Y., 2007. Molybdenum deposits in East Qinling. Earth Sci. Front. 14, 186–198 (in Chinese with English abstract).
Li, N., Chen, Y.J., Pirajno, F., Gong, H.J., Mao, S.D., Ni, Z.Y., 2012a. LA-ICP-MS zircon U-Pb dating, trace element and Hf isotope geochemistry of the Heyu granite batholith, eastern Qinling, central China: implications for Mesozoic tectono-magmatic evolution. Lithos 142–143, 34–47.
Li, N., Chen, Y.J., Pirajno, F., Ni, Z.Y., 2012b. Timing of the Yuchiling giant porphyry Mo system, and implications for ore genesis. Mineral. Deposita 48, 505–524.
Li, C.Y., Zhang, H., Wang, F.Y., Liu, J.Q., Sun, Y.L., Hao, X.L., Li, Y.L., Sun, W.D., 2012c. The formation of the Dabaoshan porphyry molybdenum deposit induced by slab rollback. Lithos 150, 101–110.
Li, H., Ye, H., Wang, X., Yang, L., Wang, X., 2014. Geology and ore fluid geochemistry of the Jinduicheng porphyry molybdenum deposit, East Qinling, China. J. Asian Earth Sci. 79, 641–654.
Liu, Y.S., Hu, Z.C., Gao, S., Günther, D., Xu, J., Gao, C.G., Chen, H.H., 2008. In situ analysis of major and trace elements of anhydrous minerals by LA-ICP-MS without applying an internal standard. Chem. Geol. 257, 34–43.
Loferski, P.J., Ayuso, R.A., 1995. Petrography and mineral chemistry of the composite Deboullie pluton, northern Maine, U.S.A.: implications for the genesis of Cu–Mo mineralization. Chem. Geol. 123, 89–105.
Lowenstern, J.B., 1994. Dissolved volatile concentrations in an ore-forming magma. Geology 22, 893–896.
Lowenstern, J.B., Mahood, G.A., Hervig, R.L., Sparks, J., 1993. The occurrence and distribution of Mo and molybdenite in unaltered peralkaline rhyolites from Pantelleria. Italy. Contrib. Mineral. Petrol. 114, 119–129.
Manning, D.A.C., 1981. The effect of fluorine on liquidus phase relationships in the system Qz-Ab-Or with excess water at 1 kb. Contrib. Mineral. Petrol. 76, 206–215.
Mao, J.W., Xie, G.Q., Bierlein, F., Qü, W.J., Du, A.D., Ye, H.S., Pirajno, F., Li, H.M., Guo, B.J., Li, Y.F., Yang, Z.Q., 2008. Tectonic implications from Re–Os dating of Mesozoic molybdenum deposits in the East Qinling-Dabie orogenic belt. Geochim. Cosmochim. Acta 72, 4607–4626.
Mao, J.W., Xie, G.Q., Pirajno, F., Ye, H.S., Wang, Y.B., Li, Y.F., Xiang, J.F., Zhao, H.J., 2010. Late Jurassic-Early Cretaceous granitoid magmatism in Eastern Qinling, central-eastern China: SHRIMP zircon U-Pb ages and tectonic implications. Aust. J. Earth Sci. 57, 51–78.
Mao, J.W., Pirajno, F., Xiang, J.F., Gao, J.J., Ye, H.S., Li, Y.F., Guo, B.J., 2011. Mesozoic molybdenum deposits in the east Qinling-Dabie orogenic belt: characteristics and tectonic settings. Ore Geol. Rev. 43, 264–293.
Mengason, M.J., Candela, P.A., Piccoli, P.M., 2011. Molybdenum, tungsten and manganese partitioning in the system pyrrhotite–Fe–S–O melt–rhyolite melt: impact of sulfide segregation on arc magma evolution. Geochim. Cosmochim. Acta 75, 7018–7030.
Mercer, C.N., Hofstra, A.H., Todorov, T.I., Roberge, J., Burgisser, A., Adams, D.T., Cosca, M., 2015. Pre-eruptive conditions of the HideawayPark Topaz Rhyolite: insights into metal source and evolution of magma parental to the Henderson Porphyry Molybdenum Deposit, Colorado. J. Petrol. 56, 645–679.
Mungall, J.E., 2002. Roasting the mantle: slab melting and the genesis of major Au and Au-rich Cu deposits. Geology 30, 915–918.
Munoz, J.L., 1984. F-OH and Cl-OH exchange in micas with applications to hydrothermal ore deposits. Rev. Mineral. Geochem. 13, 469–493.
Munoz, J.L., 1992. Calculation of HF and HClfugacities from biotite compositions: revised equations. Geol. Soc. Am. 24, 221 Abstracts with Programs.
Nash, W.P., Crecraft, H.R., 1985. Partition coefficients for trace elements in silicic magmas. Geochim. Cosmochim. Acta 49, 2309–2322.
Patiño Douce, A.E., Harris, N., 1998. Experimental constraints on Himalayan anatexis. J.

Petrol. 39, 689–710.
Piccoli, P., Candela, P., Rivers, M., 2000. Interpreting magmatic processes from accessory phases: titanite-a small-scale recorder of large-scale processes. Proc. R. Soc. Earth Sci. 91, 257–267.
Qi, Y., 2014. Petrogenesis of Laojunshan and Taishanmiao Granite Plutons in Eastern Qinling, central China (Dissertation for Master's Degree). University of Science and Technology of China, pp. 1–50 (in Chinese with English abstract).
Qiu, J.T., Yu, X.Q., Santosh, M., Zhang, D.H., Chen, S.Q., Li, P.J., 2013. Geochronology and magmatic oxygen fugacity of the Tongcun molybdenum deposit, northwest Zhejiang, SE China. Mineral. Deposita 48, 545–556.
Rasmussen, K.L., Mortensen, J.K., 2013. Magmatic petrogenesis and the evolution of (F:Cl:OH) fluid composition in barren and tungsten skarn-associated plutons using apatite and biotite compositions: case studies from the northern Canadian Cordillera. Ore Geol. Rev. 50, 118–142.
Rempel, K.U., Williams-Jones, A.E., Migdisov, A.A., 2009. The partitioning of molybdenum(VI) between aqueous liquid and vapour at temperatures up to 370 °C. Geochim. Cosmochim. Acta 73, 3381–3392.
Rieder, M., Cavazzini, G., D'yakonov, Y.S., Frank-Kamenetskii, V.A., Gottardi, G., Guggenheim, S., Koval', P.V., Mueller, G., Neiva, A.M.R., Radoslovich, E.W., Robert, J.-L., Sassi, F.P., Takeda, H., Weiss, Z., Wones, D.R., 1998. Nomenclature of the micas. Can. Mineral. 36, 905–912.
Robb, L., 2005. Introduction to Ore-Forming Processes. Blackwell Publishing, pp. 1–367.
Selby, D., Nesbitt, B.E., 2000. Chemical composition of biotite from the Casino porphyry Cu–Au–Mo mineralization, Yukon, Canada: evaluation of magmatic and hydrothermal fluid chemistry. Chem. Geol. 171, 77–93.
Shinohara, H., Kazahaya, K., Lowenstern, J.B., 1995. Volatile transport in a convecting magma column: implications for porphyry Mo mineralization. Geology 23, 1091–1094.
Shock, E.L., Sassani, D.C., Willis, M., Sverjensky, D.A., 1997. Inorganic species in geologic fluids: correlations among standard molal thermodynamic properties of aqueous ions and hydroxide complexes. Geochim. Cosmochim. Acta 61, 907–950.
Siahcheshm, K., Calagari, A.A., Abedini, A., Lentz, D.R., 2012. Halogen signatures of biotites from the Maher-Abad porphyry copper deposit, Iran: characterization of volatiles in syn- to post-magmatic hydrothermal fluids. Int. Geol. Rev. 54, 1353–1368.
Sillitoe, R.H., 2010. Porphyry Copper Systems. Econ. Geol. 105, 3–41.
Sinclair, W.D., 2007. Porphyry Deposits. Mineral Deposits of Canada: A Synthesis of Major Deposit-Types, District Metallogeny, the Evolution of Geological Provinces, and Exploration Methods. Geol. Assoc. of Canada, Mineral Deposits Division, Spec. Publ,, vol. 5. pp. 223–243.
Speer, J.A., 1984. Micas in igneous rocks. Rev. Mineral. Geochem. 13, 299–356.
Stussi, J.M., Cuney, M., 1996. Nature of biotites from alkaline, calc-alkaline and peraluminous magmas by Abdel-Fattah M. Abdel-Rahman: a comment. J. Petrol. 37, 1025–1029.
Sun, W.D., Huang, R.F., Li, H., Hu, Y.B., Zhang, C.C., Sun, S.J., Zhang, L.P., Ding, X., Li, C.Y., Zartman, R.E., 2015. Porphyry deposits and oxidized magmas. Ore Geol. Rev. 65, 97–131.
Tacker, R.C., Candela, P.A., 1987. Partitioning of molybdenum between magnetite and melt; a preliminary experimental study of partitioning of ore metals between silicic magmas and crystalline phases. Econ. Geol. 82, 1827–1838.
Tingle, T.N., Fenn, P.M., 1984. Transport and concentration of molybdenum in granite molybdenite systems: effects of fluorine and sulfur. Geology 12, 156–158.
van Middelaar, W.T., Keith, J.D., 1990. Mica chemistry as an indicator of oxygen and halogen fugacities in the CanTung and other W-related granitoids in the North American Cordillera. In: Stein, H.J., Hannah, J.L. (Eds.), Ore-bearing Granite Systems: Petrogenesis and Mineralizing Process. Geol. Soc.Am., Special Paper, vol. 246. pp. 205–220.
Walker, B.A., Miller, C.F., Lowery Claiborne, L., Wooden, J.L., Miller, J.S., 2007. Geology and geochronology of the Spirit Mountain batholith, southern Nevada: implications for timescales and physical processes of batholith construction. J. Volcanol. Geoth. Res. 167, 239–262.
Wan, Y.S., Wilde, S.A., Liu, D.Y., Yang, C.X., Song, B., Yin, X.Y., 2006. Further evidence for ~1.85 Ga metamorphism in the Central Zone of the North China Craton: SHRIMP U-Pb dating of zircon from metamorphic rocks in the Lushan area, HenanProvince. Gondwana Res. 9, 189–197.
Wang, X., Wang, T., Ke, C., Yang, Y., Li, J., Li, Y., Qi, Q., Lv, X., 2015. Nd–Hf isotopic mapping of Late Mesozoic granitoids in the East Qinling orogen, central China: constraint on the basements of terranes and distribution of Mo mineralization. J. Asian Earth Sci. 103, 169–183.
Wang, C.M., Chen, L., Bagas, L., Lu, Y.J., He, X.Y., Lai, X.R., 2016. Characterization and origin of the Taishanmiao alumious A-type granites: implications for Early Cretaceous lithoshperic thinning at the southern margin of the North China Craton. Int. J. Earth Sci. 105, 1563–1589.
Watson, E.B., Harrison, T.M., 1983. Zircon saturation revisited: temperature and composition effects in a variety of crustal magma types. Earth Planet. Sci. Lett. 64, 295–304.
Webster, J.D., 1997a. Chloride solubility in felsic melts and the role of chloride in magmatic degassing. J. Petrol. 38, 1793–1807.
Webster, J.D., 1997b. Exsolution of magmatic volatile phases from Cl-enriched mineralizing granitic magmas and implications for ore metal transport. Geochim. Cosmochim. Acta 61, 1017–1029.
Wones, D.R., Eugster, H.P., 1965. Stability of biotite - experiment, theory, and application. Am. Mineral. 50, 1228–1272.
Wu, G., Chen, Y., Li, Z., Liu, J., Yang, X., Qiao, C., 2014. Geochronology and fluid inclusion study of the Yinjiagou porphyry–skarn Mo–Cu–pyrite deposit in the East Qinling orogenic belt, China. J. Asian Earth Sci. 79, 585–607.
Xu, X.S., Griffin, W.L., Ma, X., O'Reilly, S.Y., He, Z.Y., Zhang, C.L., 2009. The Taihua group on the southern margin of the North China craton: further insights from U-Pb ages and Hf isotope compositions of zircons. Mineral. Petrol. 97, 43–59.
Yang, X.M., 2012. Sulphur solubility in felsic magmas: implications for genesis of intrusion-related gold mineralization. Geosci. Can. 39, 17–32.
Yang, X.M., Lentz, D.R., 2005. Chemical composition of rock-forming minerals in gold-related granitoid intrusions, southwestern New Brunswick, Canada: implications for crystallization conditions, volatile exsolution, and fluorine-chlorine activity. Contrib. Mineral. Petrol. 150, 287–305.
Yang, L., Chen, F.K., Liu, B.X., Hu, Z.P., Qi, Y., Wu, J.D., He, J.F., Siebel, W., 2013a. Geochemistry and Sr–Nd–Pb–Hf isotopic composition of the Donggou Mo-bearing granite porphyry, Qinling orogenic belt, central China. Int. Geol. Rev. 55, 1261–1279.
Yang, Y., Chen, Y.J., Zhang, J., Zhang, C., 2013b. Ore geology, fluid inclusions and four-stage hydrothermal mineralization of the Shangfanggou giant Mo–Fe deposit in Eastern Qinling, central China. Ore Geol. Rev. 55, 146–161.
Yang, Y.F., Chen, Y.J., Pirajno, F., Li, N., 2015. Evolution of ore fluids in the Donggou giant porphyry Mo system, East Qinling, China, a new type of porphyry Mo deposit: evidence from fluid inclusion and H-O isotope systematics. Ore Geol. Rev. 65, 148–164.
Ye, H.S., Mao, J.W., Li, Y.F., Guo, B.J., Zhang, C.Q., Liu, J., Yan, Q.R., Liu, G.Y., 2006. SHRIMP zircon U-Pb and molybdenite Re-Os dating for the superlarge Donggou porphyry Mo deposit in East Qinling, China, and its geological implication. Acta Geol. Sinica 80, 1078–1088 (in Chinese with English abstract).
Ye, H.S., Mao, J.W., Xu, L.G., Gao, J.J., Xie, G.Q., Li, X.Q., He, C.F., 2008. SHRIMP zircon U-Pb dating and geochemistry of the Taishanmiao alumious A-type granite in western HenanProvince. Geol. Rev. 54, 699–711 (in Chinese with English abstract).
Zajacz, Z., Halter, W.E., Pettke, T., Guillong, M., 2008. Determination of fluid/melt partition coefficients by LA-ICPMS analysis of co-existing fluid and silicate melt inclusions: controls on element partitioning. Geochim. Cosmochim. Acta 72, 2169–2197.
Zhang, W., Lentz, D.R., Thorne, K.G., McFarlane, C., 2016. Geochemical characteristics of biotite from felsic intrusive rocks around the Sisson Brook W-Mo–Cu deposit, west-central New Brunswick: an indicator of halogen and oxygen fugacity of magmatic systems. Ore Geol. Rev. 77, 82–96.
Zhao, T.P., Zhai, M.G., Xia, B., Li, H.M., Zhang, Y.X., Wan, Y.S., 2004. Zircon U-Pb SHRIMP dating for the volcanic rocks of the Xiong'er Group: constraints on the initial formation age of the cover of the North China Craton. Chin. Sci. Bull. 49, 2495–2502.
Zhu, C., Sverjensky, D.A., 1991. Partitioning of F-Cl-OH between minerals and hydrothermal fluids. Geochim. Cosmochim. Acta 55, 1837–1858.
Zhu, C., Sverjensky, D.A., 1992. F-Cl-OH partitioning between biotite and apatite. Geochim. Cosmochim. Acta 56, 3435–3467.
Zhu, L., Ding, Z., Yao, S., Zhang, G., Song, S., Qu, W., Guo, B., Lee, B., 2009. Ore-forming event and geodynamic setting of molybdenum deposit at Wenquan in Gansu Province, Western Qinling. Chin. Sci. Bull. 54, 2309.